Flow Visualization Studies of the Mach Number Effects on Dynamic Stall of an Oscillating Airfoil

M. S. Chandrasekhara*
Naval Postgraduate School, Monterey, California
and
L. W. Carr†
NASA Ames Research Center, Moffett Field, California

Compressibility effects on dynamic stall of a NACA 0012 airfoil undergoing sinusoidal oscillatory motion were studied using a stroboscopic schlieren system. Schlieren pictures and some quantitative data derived from them are presented and show the influence of freestream Mach number and reduced frequency on the dynamic stall vortex. This study shows that a dynamic stall vortex *always* forms and convects over the airfoil upper surface at approximately 0.3 times the freestream velocity for all cases studied. The results also demonstrate that occurrence of deep stall is delayed to higher angles of attack with increased reduced frequency, even when compressibility effects are present, but increasing Mach number alone has the opposite effect.

Nomenclature

c = airfoil chord
f = frequency of oscillation, Hz
k = reduced frequency, $= \pi fc/U_\infty$
M = freestream Mach number
U_∞ = freestream velocity
U_{DSV} = dynamic stall vortex convection velocity
x = chordwise distance
α = angle of attack
α_0 = mean angle of attack
α_m = amplitude of oscillation
ω = circular frequency, rad/s

I. Introduction

DYNAMIC stall delay and the unsteady lift augmentation due to it have been the subject of considerable research during the past 15 years. The presence of dynamic stall on the retreating blade of helicopters has significantly limited the performance of these vehicles; in contrast, the dynamic lift increase associated with rapid pitching motion can improve the agility of fighter aircraft. The reader is referred to the comprehensive reviews of research in this area by Carr[1] and McCroskey[2] for an evaluation of past efforts; the present paper will focus primarily on the effects of Mach number on the stall process.

As the required flight envelopes of both helicopters and fixed wing aircraft are expanded, it has become apparent that freestream Mach number plays an increasing role in the dynamic stall process. There is strong evidence that as the Mach number increases, the dynamic stall delay decreases; in fact, there are indications that the dynamic lift overshoot on aircraft wings is virtually eliminated as the Mach number exceeds 0.6.[3] This decrease in overshoot has also been observed for helicopter airfoils oscillating in pitch by Dadone.[4] Lorber and Carta[5] have recently observed this effect in tests of airfoils performing oscillatory as well as constant pitch rate motions.

However, all of these studies measured the effects of dynamic stall by use of surface mounted gages such as pressure transducers and skin friction sensors or by measuring the integrated lift, drag, and pitching moment; no visualization of the global flowfield has been published for compressible flow conditions. In fact, little quantitative information has been obtained concerning the details of the dynamic stall vortex itself at the Mach numbers representative of the flow on helicopters or aircraft in flight. The global characteristics of dynamic stall in incompressible flow have been documented by several researchers (see Carr[1] for a review). However, it is clear that the flow mechanisms which induce the stall delay can change as the freestream Mach number increases; for example, an airfoil experiencing trailing-edge stall at low speeds can experience leading-edge stall as the freestream Mach number is increased.[6]

As the Mach number increases beyond 0.2, the local flow around the leading edge can become supersonic[6] (Fig. 1). When supersonic velocities occur over the airfoil in steady flow, a shock usually forms. If a shock appears in unsteady

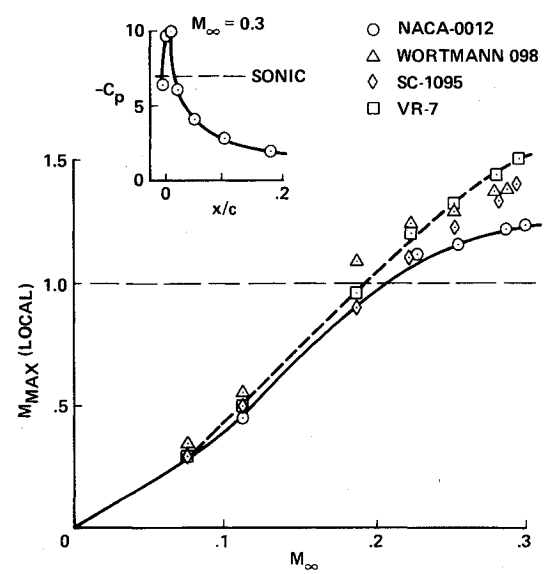

Fig. 1 Local Mach number on leading edge of an oscillating airfoil vs freestream Mach number.

Presented as Paper 89-0023 at the AIAA 27th Aerospace Sciences Meeting, Reno, NV, Jan. 9-12, 1989; received March 27, 1989; revision received Jan. 4, 1990.

*Assistant Director and Adjunct Professor, Navy-NASA Institute of Aeronautics. Associate Fellow AIAA.

†Research Scientist, Aeroflightdynamics Directorate, U.S. Army ARTA, and Fluid Dynamics Research Branch, NASA. Member AIAA.

flow, it could dramatically affect the dynamic stall process. Although there has been no direct experimental evidence to substantiate the presence of the shock on a dynamically stalling airfoil, calculations by Visbal,[7] Carr et al.,[8] and Fung and Carr[9] indicate its presence near the location of peak suction pressure. Thus, to exploit the benefits of dynamic delay of stall, a much better understanding of the formation and behavior of the dynamic stall vortex at high flight speeds is needed. One of the first steps toward this goal is to produce high quality flow visualization at high subsonic velocities. Since the velocities are high and the flow is largely separated and turbulent, most methods of flow visualization will not work satisfactorily. The research discussed in this paper presents a novel approach to obtaining this important experimental information. The paper describes the dynamic stall process using a stroboscopic schlieren method, which documents the vortex characteristics for a range of Mach numbers and reduced frequencies. Resulting analyses of the images show that compressibility has a direct impact on dynamic stall.

II. Description of the Facility, Instrumentation, and Technique

The experiments were conducted in the newly built Compressible Dynamic Stall Facility (CDSF). The CDSF is an in-draft wind tunnel with a 25×35-cm test section, driven by a compressor, which is connected to the tunnel exit throat (for details see Ref. 10). The compressor maintains a vacuum pressure sufficient to create sonic velocity at the throat downstream of the test section. The tunnel velocity is controlled by varying the area of this throat.

The uniqueness of the CDSF is that it has been specifically designed for dynamic stall flow visualization studies at high speeds. Unobstructed viewing of the complete flowfield surrounding the airfoil during unsteady motion is possible in the facility. This allows unobstructed qualitative as well as quantitative nonintrusive diagnosis of the instantaneous unsteady flow conditions that occur during dynamic stall. To achieve this, the airfoil is simply supported by pins between two 2.54-cm-thick optical quality glass windows. The pins are smaller than the local airfoil thickness so that there is no obstruction of the airfoil contour by the support mechanism. The window/ airfoil combination is driven in sinusoidal oscillation by a 4-bar, push-rod-flywheel system, about the 25% chord point as shown in Fig. 2. The drive motor is a variable speed ac motor with a controller to maintain speed to within 1%. The clearance between the airfoil and the window is about 0.15 mm. A thin, circular, rubber cushion separates the glass windows from the airfoil to prevent the danger of breaking the windows due to impact of the airfoil, should any lateral movement occur during oscillation. The airfoil is pinned at 25 and 70% chord.

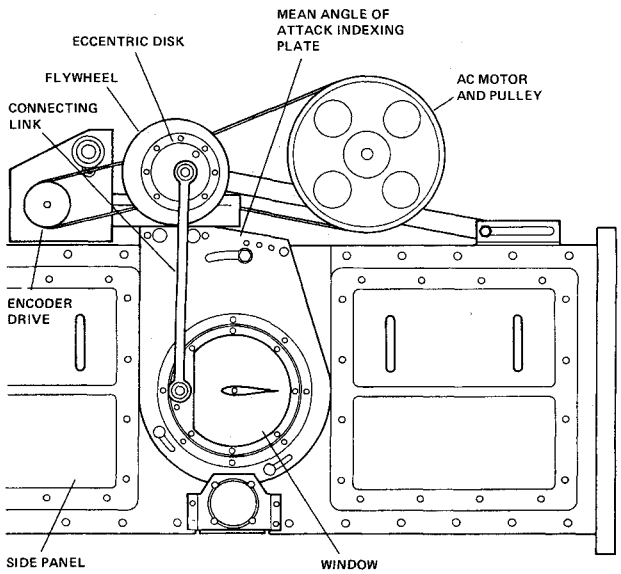

Fig. 2 Schematic of the CDSF test section.

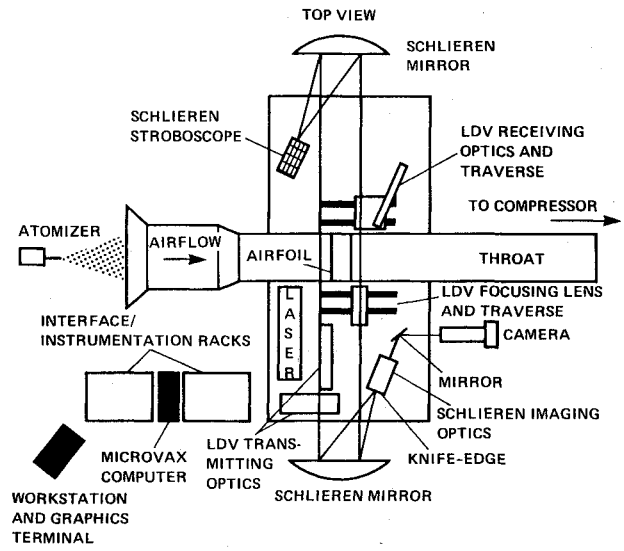

Fig. 3 Schematic of the CDSF and instrumentation.

Three encoders are used to register the mean angle of attack, the instantaneous amplitude of oscillation, and the phase angle/frequency information. The drive mechanism can oscillate the airfoil at frequencies of up to 100 Hz with oscillatory amplitudes ranging from 2 to 10 deg. The mean angle of attack can be varied from 0 to 15 deg.

Flow visualization was obtained using a stroboscopic schlieren system (see Fig. 3). A xenon arc lamp (EG&G, Inc., Model 1P-1, 1 mm arc length) was used as the light source; an iris diaphragm set at 0.5 mm was located in front of the light source and served to form a point source. The aperture was located at the focal point of a 45-cm-diam, 3-m-focal-length concave mirror used to produce a parallel cylinder of light, which after passing through the test section was focused by another concave mirror onto a vertical knife edge. The light that passed the knife edge was focused by a lens and directed to the photographic focal plane by a plane mirror.

The strobe was triggered electronically at appropriate phase angles with custom built hardware using the output of the phase angle encoder. The light source could be pulsed either once for freeze action studies or any number of times for movies. In addition, this circuit could also be controlled by a computer. The circuit recycled rapidly and could trigger the strobe light at the highest frequency of interest (100 Hz). In practice, the phase angle was selected from the front panel switches. The actual phase angle at which the strobe was pulsed was displayed on the panel to serve as a check on the operation of the circuit. The flash duration was about 1.5 μs.

The experiment consisted of taking single exposure photographs on Polaroid type 52 film at the desired phase angle for the matrix of test conditions presented in Table 1. In each run, the presence of the dynamic stall vortex was determined visually, and pictures were taken at close phase intervals to study the dynamic stall development. Additional pictures were taken throughout the complete cycle.

A. Test Conditions

The range of Mach number and reduced frequency was chosen to encompass the conditions that occur on the retreating blade of helicopter rotors in forward flight. The specific tests were performed at the conditions shown in Table 1. The experimental conditions were $0.15 \leq M \leq 0.45$, $0 \leq k \leq 0.1$ with the angle of attack $\alpha = \alpha_0 q_m + \sin\omega t$ with $\alpha_0 = \alpha_m = 10$ deg. The airfoil was NACA 0012 with 7.62-cm chord.

Table 1 Experimental conditions

M	k						
	0	0.0125	0.025	0.05	0.075	0.1	0.15
0.15	—	—	—	X	—	X	X
0.20	X	—	—	X	X	X	—
0.25	X	X	X	X	X	X	—
0.30	X	X	X	X	X	X	—
0.35	X	X	X	X	X	—	—
0.40	X	—	X	X	—	—	—
0.45	X	—	X	X	—	—	—

III. Results and Discussion

In this section, schlieren photographs are presented at selected angles as the airfoil undergoes one cycle of oscillation. A discussion of these photographs is followed by discussion of the effects of Mach number and reduced frequency and an evaluation of the convection velocity of the dynamic stall vortex.

A. Stroboscopic Schlieren Studies

Unlike other flow visualization methods that show the streamline or streakline patterns that integrate the past history of the flow, the schlieren technique enables instantaneous visualization of the flow. Each picture is a "snapshot" of the flow at the instant the photograph is taken and shows the influence of the vortex on the flowfield only at that time. Most published schlieren data are for flows with very strong density gradients, such as shock waves, which are highly visible. In the present experiment, the system was intentionally set to be very sensitive so that weak density gradients could be made visible. It was possible to photograph the density gradient in the separated flow past a stationary airfoil at $M=0.1$ with this system. It should be noted that, except near the leading edge, the density gradients are very small in the range of Mach numbers for which the experiments were conducted; even so, the dynamic stall vortex is clearly visible.

Some notes of caution are appropriate: at certain phase angles, the leading edge of the airfoil appears to be in its own shadow, and a ghost image can be seen in some photographs. The exact cause of this is not yet known; but it is suspected to be due to a slight misalignment of the system at some window angles because it appears at the same angles for all flow cases studied and is independent of the flow. Also, the thin streaks that appear perpendicular to the airfoil on the upper and lower surfaces at 70% chord are due to cracks in the glass that appeared when the airfoil pins were being push fitted into matching holes in the glass windows. Fortunately, the cracks did not propagate during the experiments.

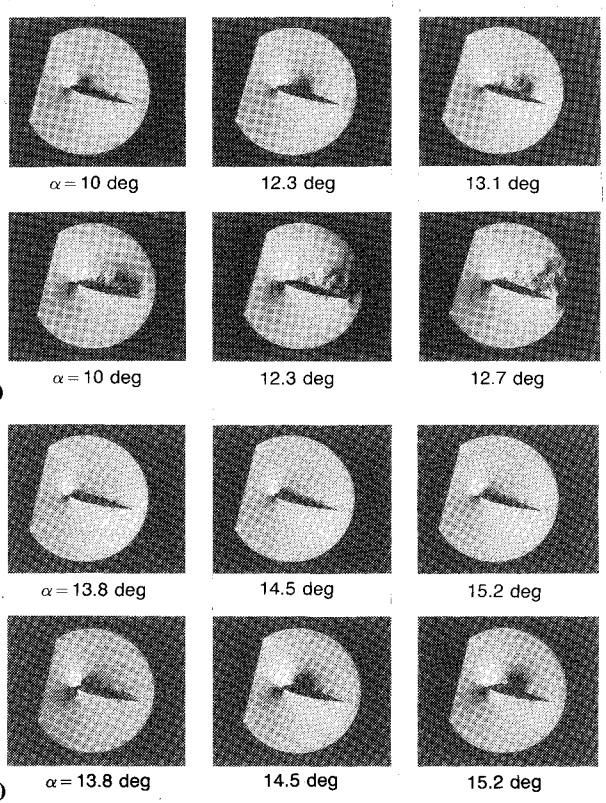

Fig. 4 Comparison of the effect of Mach number on dynamic stall process; a) $M=0.3$, $k=0.05$, b) $M=0.4$, $k=0.05$.

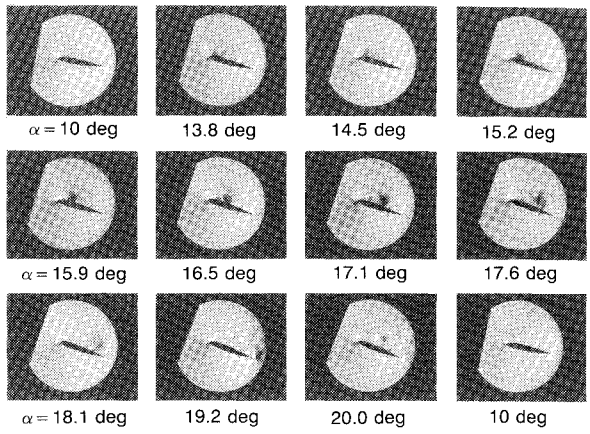

Fig. 5a Stroboscopic schlieren photographs of the compressibility effects on dynamic stall of an oscillating airfoil: $M=0.2$, $k=0.1$, $\alpha=10+10\sin(\omega t)$.

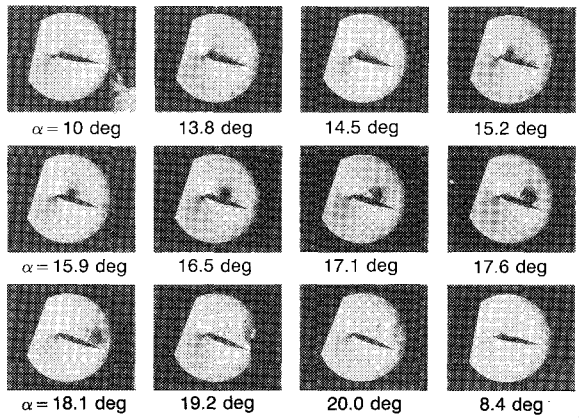

Fig. 5b Stroboscopic schlieren photographs of the compressibility effects on dynamic stall of an oscillating airfoil: $M=0.3$, $k=0.1$, $\alpha=10+10\sin(\omega t)$.

Schlieren photographs for several test conditions are presented in Fig. 4. They show the flow gradients at selected angles of attack for $M=0.3$ and 0.4 for a fixed reduced frequency of 0.05. As can be seen from Fig. 4a ($M=0.3$) and Fig. 4b ($M=0.4$), dynamic stall occurs at lower angles of attack for higher Mach numbers. At $M=0.3$, the stall angle of attack is 15.9 deg and at $M=0.4$, it is 14.5 deg. Conversely, at an angle of attack of 14.5 deg while the dynamic stall vortex remains on the surface and has progressed only to about 70% of the chord at $M=0.3$, it has already been shed into the wake at $M=0.4$.

Figure 5 presents flow visualization pictures through a half cycle of oscillation consisting of pitchup from a mean angle of 10 deg to the maximum angle of 20 deg and then pitch down to 10 deg for $M=0.2$ (Fig. 5a) and $M=0.3$ (Fig. 5b) for $k=0.1$. The approximate location of the vortex core compares very well for both cases, establishing the independence of the process of dynamic stall formation up to $M=0.3$. Interpretation of the schlieren photographs at these low freestream Mach numbers can only be approximate in nature. However, the following observations can be made from the series of photographs in Fig. 5.

1) The dark region around the leading edge on the lower surface is the density gradient field associated with the stagnation region. Its size and location change with the angle of attack.

2) The density gradient field in the acceleration region near the leading edge and beyond appears as a white patch above the upper surface. As is well known, the suction peak, measured at the surface of airfoils, is found near the leading edge at angles of attack similar to those seen here. Since the effect of the suction peak (which is a surface measurement) on the flow away from the surface could not be clearly identified in these photographs optimized for dynamic stall vortex visualization, inverse schlieren pictures were obtained for the same angles at the same conditions by reversing the knife edge (i.e., positive gradients as bright and vice versa) for a few cases (not shown). These clearly showed that the density gradient associated with the suction peak was within the first 2% of the chord. The region itself is about 1/2% chord wide. Also, because the density gradient field is inherently different from the static pressure field due to compressibility effects, care is needed in interpreting the pictures. The density gradients away from the surface, as revealed in the schlieren photographs, agree very well with the calculations of this flow using Navier-Stokes codes.[11] Following the white patch, a dark region appears in which the density gradients have magnitudes similar to those in the stagnation region. The dark region appears at lower angles of attack as the Mach number is increased, reflecting the increased density gradients which result from the higher flow speed.

3) The vorticity developed over the leading-edge region coalesces into a vortex, which first appears as the dynamic stall vortex at approximately 15–20% chord. Unfortunately, the exact origin of the dynamic stall vortex is hard to separate from the density variations produced by the decelerating flow on the airfoil. However, the location at which this process is complete (and the vortex begins to move over the surface) can be determined from the photographs and is found to depend on the Mach number and reduced frequency. This location occurs further downstream with increasing Mach number but further upstream with increasing reduced frequency. During the coalescence process, the vorticity generated near the leading edge is consolidated, and the dynamic stall vortex fully forms at about 20% chord. It should be noted that by the time this happens, there is no additional (useful) vorticity input to the flow. The airfoil experiences leading-edge stall, which can be seen clearly in the schlieren pictures as a white streak that originates at the leading edge. The vorticity that is generated is due to the extremely rapid accelerations generated here (see Ref. 12) and thus is indirectly due to pressure gradients. Once leading-edge separation occurs, this effect is lost. Considerable thickening of the boundary layer occurs by the time the vortex has fully formed. This phenomenon is nearly the same at all Mach numbers and reduced frequencies.

4) As the airfoil continues to pitch up toward its maximum amplitude (20 deg), the dynamic stall vortex begins to convect downstream and eventually lifts off the surface and is shed into the wake. The angle at which the vortex is released (occurrence of deep stall) from the surface or is convected past the trailing edge is strongly dependent upon the Mach number and reduced frequency (summarized in Table 2 along with the static stall angle). As the Mach number is increased, deep stall occurs at lower angles of attack. As the reduced frequency is increased, the vortex remains on the upper surface until reaching higher angles of attack. All of these angles are considerably higher than the static stall angles at the corresponding Mach numbers. During the deep stall phase, a vorticity layer can still be seen to separate the outer potential flow from the inner viscous layer.

5) During the downward motion of the airfoil, the flow starts to reattach at about 10 deg, and the reattachment is complete between angles of attack 10 and 9 deg. Reattachment appears to be only a weak function of the parameters of this experiment.

6) At angles of incidence below 10 deg (or the reattachment angle), no significant unsteady effects are present.

7) In many instances, trailing-edge vortices and vortices in the separated shear layer can be identified. However, these do

Table 2 Vortex release angle of attack

M	k						
	0[a]	0.0125	0.025	0.05	0.075	0.1	0.15
0.15	——	——	——	——	——	18.1	19.5
0.20	——	——	——	15.9	17.1	18.3	——
0.25	——	13.8	14.5	15.9	17.1	18.1	——
0.30	12.4	13.4	14.1	15.9	17.6	18.1	——
0.35	11.6	——	13.8	15.2	15.9	——	——
0.40	10.8	——	13.1	14.5	——	——	——
0.45	9.5	——	12.3	14.2	——	——	——

[a]Best estimate of static stall angle from schlieren pictures.

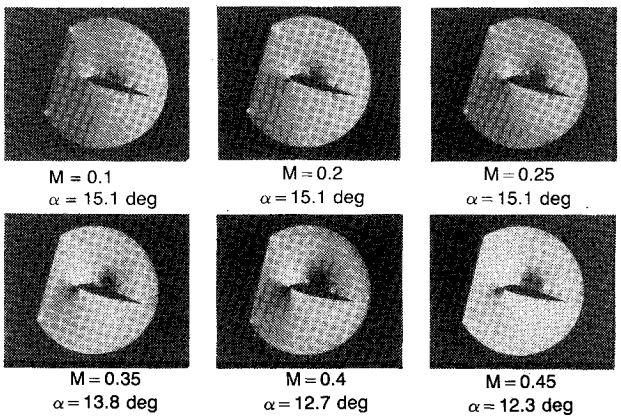

Fig. 6 Effect of compressibility on dynamic stall of an oscillating airfoil: $k = 0.05$.

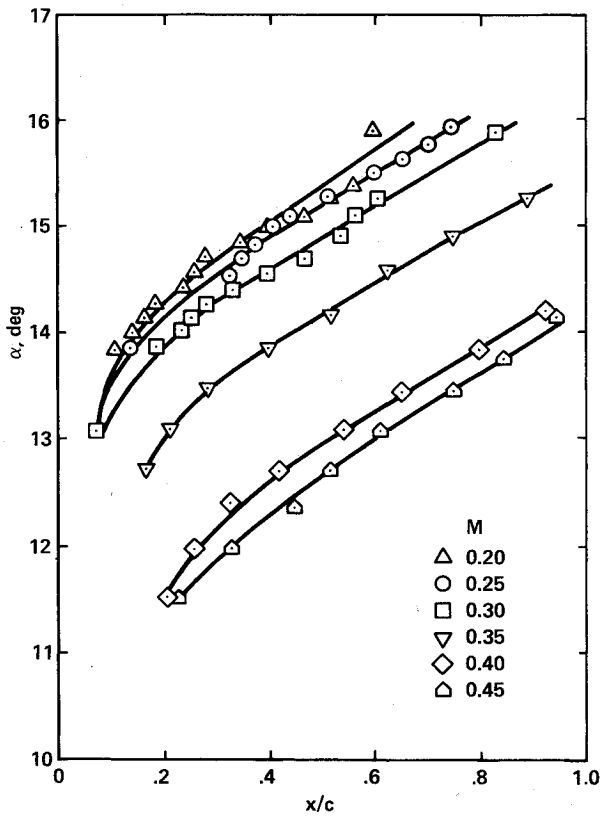

Fig. 7 Quantitative effects of Mach number on dynamic stall process: $k = 0.05$.

not appear to have any effect on the dynamic stall vortex or the process of its formation and passage down the airfoil surface.

8) No shocks could be identified in any of the conditions studied to date. However, the present schlieren system has been set up to visualize the global flowfield. A shock, if present, is suspected to be very small (about 1 mm high) and located between 0–5% chord. Also, the spanwise averaging effect of the schlieren technique may smear it. Future investigations are expected to reveal these flow details.

B. Quantitative Effects of Compressibility

Although no shocks have been documented, the effects of compressibility are clearly shown in Fig. 6, in which pictures of the dynamic stall vortex at about 50% chord location are presented for $M=0.1$, 0.2, 0.25, 0.35, 0.40, and 0.45. The angle of attack for a fixed vortex location remains constant until $M=0.3$. This behavior indicates that stall occurred earlier in the cycle at higher Mach numbers.

The location of the dynamic stall vortex, measured from the schlieren photographs, is plotted in Fig. 7 for $k=0.05$ at different points in the cycle for different Mach numbers. The most striking feature is that up to $M=0.25$, the vortex locations are nearly identical. For $M\geq 0.25$, rapid departures appear and as the Mach number is increased, the stall vortex begins to appear at dramatically lower phase angles (angles of attack). $M=0.25$–0.3 seems to be the demarkation between subcritical and supercritical flow over the airfoil. Thus, compressibility has a first-order effect on the process of dynamic stall causing it to occur at lower angles of attack. This is the

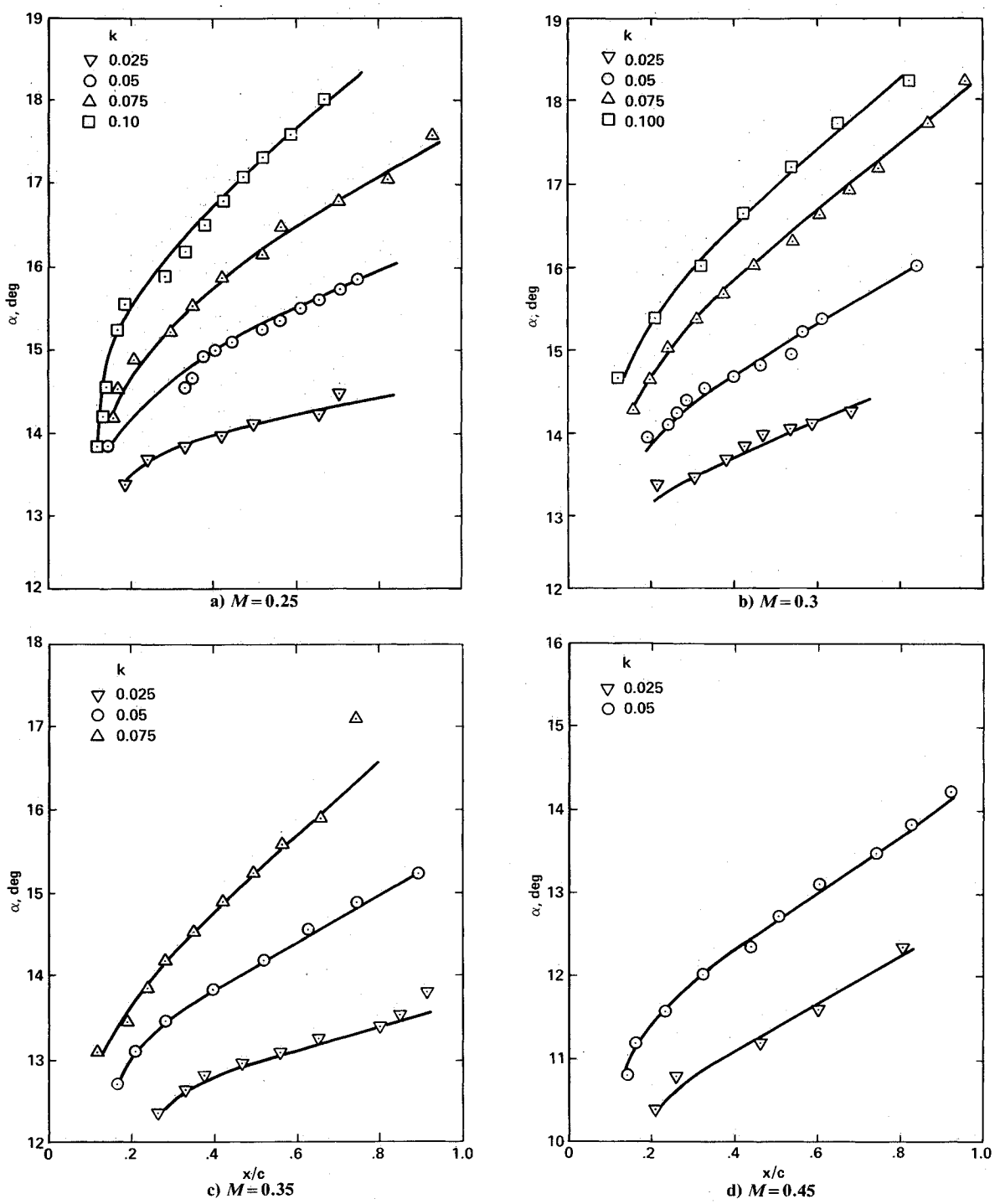

Fig. 8 Effects of reduced frequency on dynamic stall.

first visual evidence (at flight Mach numbers) that the global characteristics of the dynamic stall vortex are sensitive to Mach number.

In the present experiments, the Reynolds number was increased by a factor of 3 during the tests for $M=0.1$–0.3. The Reynolds number for the whole experiment ranged from 2 to 9×10^5. This did not affect the formation or the convection of the dynamic stall vortex, as can be seen from Fig. 7. However, the figure shows that a marked departure in the loci of the vortex locations appears for $M\geq0.3$. Thus, the trend seen is very clearly due to compressibility effects only.

Another interesting feature can also be seen from Fig. 7. Once again, beginning at $M=0.3$, departures in the development of the dynamic stall vortex occur. The point where it can be clearly detected moves further downstream from the leading edge with increasing Mach number. The reason for this is not clear at this time. It is theorized that the local supersonic flow plays an important role in the process of vortex formation, which includes the assimilation of the vorticity into the vortex. Although the vortex does indeed form at all Mach numbers, it appears that the vortex is weaker at higher Mach numbers, as evidenced by it being convected past the trailing edge at much lower angles of attack. The following heuristic reasoning may be offered for this: the flow separates at a lower angle of attack, and at this condition, the curvature of the streamlines near the leading edge is smaller and hence the pressure gradient is reduced. Thus, the net vorticity introduced is smaller, which leads to the conclusion that the vortex should be weaker.

C. Quantitative Effects of Reduced Frequency

As just discussed, the effect of increasing the reduced frequency is to keep the dynamic stall vortex on the surface to higher angles of attack. This can be seen more clearly in Fig. 8 for Mach numbers ranging from 0.25 to 0.45. In fact for $k=0.1$ and $M=0.20$, the vortex remains on the surface for angles as high as 18.1 deg.

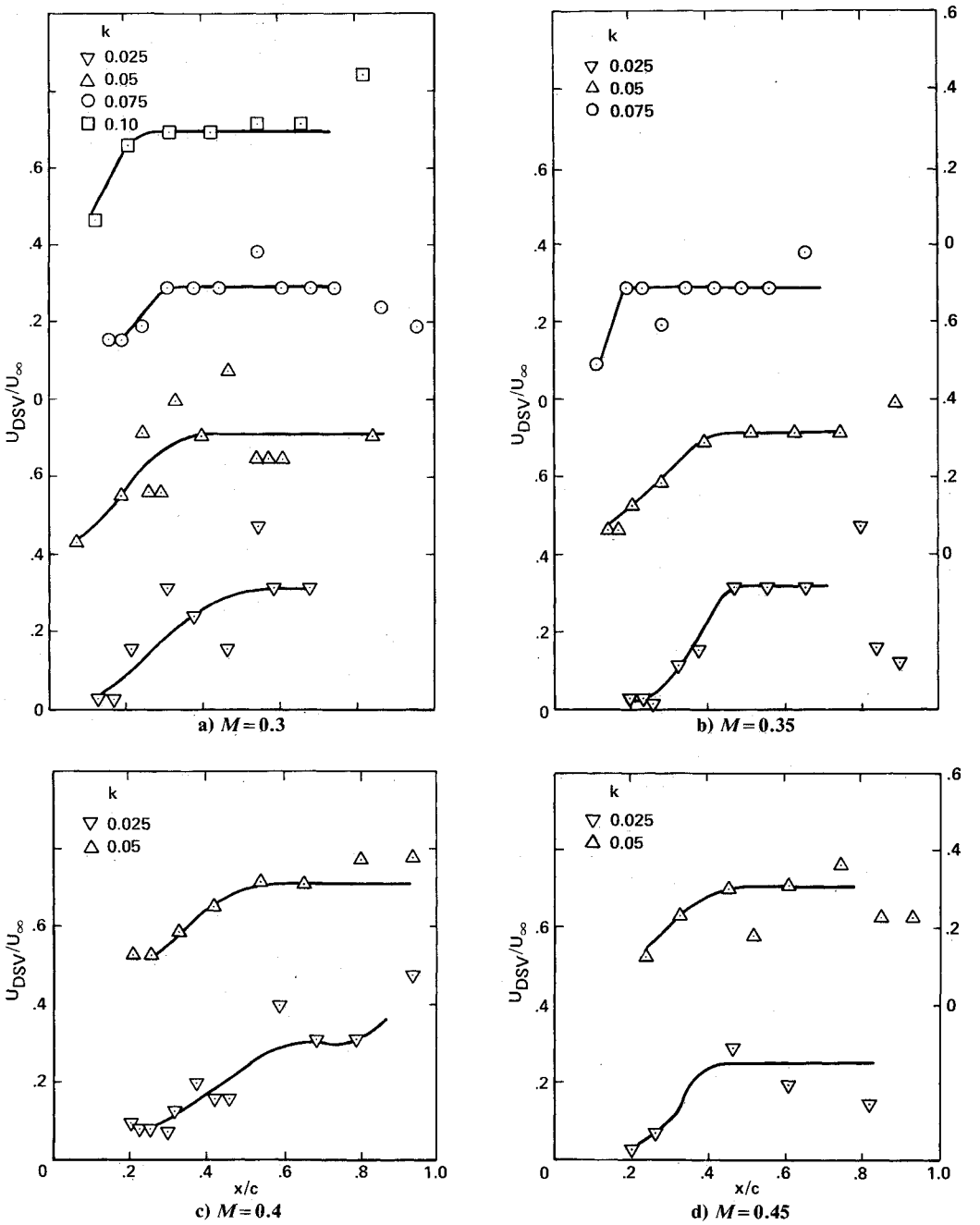

Fig. 9 Convection velocity of the dynamic stall vortex.

Once again, $M=0.3$ is the freestream condition when compressibility effects appear. Of most interest is the appearance of the dynamic stall vortex (or at least, its impression on the schlieren) closer to the leading edge as the reduced frequency is increased. The exact mechanism of the creation of the vortex is still not known. Its understanding will require a careful study of the events near the leading edge. But it is hoped that the following ideas will be of some use in this context. The discussions presented by Reynolds and Carr[12] explain how the motion of the body causes significant vorticity to be input into the flow depending on the pressure gradient created near the leading edge. Hence, regardless of whether there is a laminar or turbulent separation, or reattachment, or shocks, the vorticity input to the viscous layer eventually forms a vortex. The tightness with which this vortex coils and its growth during its passage on the airfoil surface is dependent on various factors, including the state of the boundary layer, and the pressure field induced on the airfoil due to a combination of Mach number and reduced frequency. Nevertheless, the stall vortex does form for all conditions studied so far.

D. Convection Velocity of Dynamic Stall Vortex

Another quantity of interest is the velocity with which the dynamic stall vortex convects over the airfoil. Since the dynamic stall vortex is clearly discernible in the photographs, it was possible to quantify the vortex velocity U_{DSV} simply by measuring its location for any two consecutive phase angles and dividing the distance traveled by the time difference for the corresponding phase angles. Since the determination of the vortex core is somewhat subjective, scatter is inevitable in the data recovered from the pictures. Despite this limitation, some interesting results emerged from such an analysis and are discussed below.

In Figs. 9a–9d, the convection velocities are plotted as a percentage of the freestream velocity for $M=0.25$ to 0.45 at different reduced frequencies. It is very clear from these that regardless of the Mach number or reduced frequency, there exists a plateau at $U_{DSV}/U_\infty=0.3$ indicating that over most of the airfoil surface, the vortex moves at a constant velocity of $0.3U_\infty$. It is interesting to note that the vortex passage speed agrees reasonably with the numbers quoted by Lorber and Carta[5] and Ericsson and Reding.[13] Three regions can be identified for all cases investigated: 1) A region where the dynamic stall vortex forms and gathers strength, 2) a region where it convects along the surface and grows at the same time, and 3) a region where it grows rapidly and lifts off into the stream.

The character of these three regions depends on the flow parameters, with region 2 becoming broader with increased reduced frequencies. For example, at $M=0.3$ for $k=0.025$, the plateau begins at $x/c=0.5$; for $k=0.05$, it begins at 0.4; and for $k=0.1$, it begins at 0.25. Somewhere beyond the 75% chord point, the vortex is released into the wake. No clear trends could be observed for this event. Since the amount of vorticity input into the flow near the leading edge is a strong function of the reduced frequency, the preceding result suggests that the vortex becomes organized "faster" (i.e., at a station closer to the leading edge) as the frequency increases.

IV. Conclusions

1) The dynamic stall vortex is present at all Mach numbers and reduced frequencies tested. Only its strength and initiation angle appear to differ with Mach number.

2) Increasing the reduced frequency helps in retaining the dynamic stall vortex on the airfoil surface to higher angles of attack, even at the highest Mach numbers tested.

3) Compressibility effects are significant beyond $M=0.3$. Dynamic stall occurs at dramatically lower angles of attack as the Mach number exceeds 0.3.

4) The dynamic stall vortex convects at a constant velocity of $0.3U_\infty$.

5) The origin of the vortex is not clear from the Schlieren images obtained during the test.

6) No shocks could be seen near the leading edge in the cases studied.

Acknowledgments

This work was initiated by the late Professor Satya Bodapati, who was instrumental in developing the unsteady aerodynamics program in the Navy-NASA Joint Institute of Aeronautics. The project was funded by ARO-MIPR-137-86 (monitored by Dr. T. Doligalski). Additional support was provided by AFOSR-MIPR-88 (monitored by Capt. H. Helin) and NAVAIR (monitored by NAVAIR T. Momiyama). The technical support of Michael J. Fidrich and the staff of the NASA Fluid Mechanics Laboratory is greatly appreciated.

References

[1]Carr, L. W., "Progress in Analysis and Prediction of Dynamic Stall," *Journal of Aircraft,* Vol. 25, No. 1, 1988, pp. 6–17.

[2]McCroskey, W. J., "The Phenomenon of Dynamic Stall," NASA TM-81264, March 1981.

[3]Harper, P. W., and Flanigan, R. E., "The Effect of Change of Angle of Attack on the Maximum Lift of a Small Model," NACA TN-2061, March 1950.

[4]Dadone, L. U., "Two-Dimensional Wind Tunnel Test of an Oscillating Rotor Airfoil," NASA CR-2914, 1977.

[5]Lorber, P. F., and Carta, F. O., "Unsteady Stall Penetration Experiments at High Reynolds Number," United Technologies Research Center Rept. R87-956930-3, April 1987.

[6]McCroskey, W. J., McAlister, K. W., Carr, L. W., Pucci, S. L., Lambert, O., and Indergrand, R. F., "Dynamic Stall on Advanced Airfoil Sections," *Journal of American Helicopter Society,* July 1981, pp. 45–50.

[7]Visbal, M. R., "Effect of Compressibility on Dynamic Stall of a Pitching Airfoil," AIAA Paper 88-0132, Jan. 1988.

[8]Carr, L. W., Platzer, M. F., Chandrasekhara, M. S., and Ekaterinaris, J. A., "Experimental and Computational Studies of Dynamic Stall," *Proceedings of the Fourth Symposium on Numerical and Physical Aspects of Aerodynamic Flows,* Springer-Verlag, New York, 1989, Chap. 15.

[9]Fung, K. Y., and Carr, L. W., "An Analytical Study of Compressibility Effects on Dynamic Stall," *Proceedings of the Ist National Fluid Mechanics Conference,* Pt. 2, 1988, pp. 799–805.

[10]Carr, L. W., and Chandrasekhara, M. S. "Design and Development of a Compressible Dynamic Stall Facility," AIAA Paper 89-0647, Jan. 1989.

[11]Chandrasekhara, M. S., Ekaterinaris, J. A., and Carr, L. W., "Experimental and Computational Studies of the Dynamic Stall Vortex," *Bulletin of the American Physical Society,* Vol. 33, 1988, pp. 2251.

[12]Reynolds, W. C., and Carr, L. W., "Review of Unsteady, Driven, Separated Flows," AIAA Paper 85-0527, March 1985.

[13]Ericsson, L. E., and Reding, J. P., "Fluid Mechanics of Dynamic Stall, Pt. I. Unsteady Flow Concepts," *Journal of Fluids and Structures,* Vol. 2, 1988, pp. 1–33.